(2) W. W. Graessley, *Adv. Polym. Sci.*, **16**, 1 (1974).
(3) J. D. Ferry, "Viscoelastic Properties of Polymers", 3rd ed., Wiley, New York, 1980.
(4) H. L. Hsieh, *J. Polym. Sci., Part A*, **3**, 153 (1965).
(5) Z. Xu, N. Hadjichristidis, J. M. Carella, and L. J. Fetters, *Macromolecules*, **16**, 925 (1983).
(6) H. Rachapudy, G. G. Smith, V. R. Raju, and W. W. Graessley, *J. Polym. Sci., Polym. Phys. Ed.*, **17**, 1211 (1979).
(7) R. S. Silas, J. Yates, and V. Thornton, *Anal. Chem.*, **31**, 529 (1959).
(8) Y. Tanaka, Y. Takeuchi, and M. Tadakoro, *J. Polym. Sci., A-2*, **9**, 43 (1971).
(9) T. M. Krigas, J. M. Carella, M. J. Struglinski, F. C. Schilling, B. Crist, and W. W. Graessley, manuscript in preparation.
(10) R. Popli and L. Mandelkern, *Polym. Bull.*, **9**, 260 (1983).
(11) J. Brandrup and E. H. Immergut, Eds., "Polymer Handbook", Wiley, New York, 1975.
(12) J. F. Saunders, R. H. Valentine, and J. D. Ferry, *J. Polym. Sci., Part A-2*, **6**, 967 (1965).
(13) D. W. Van Krevelen, "Properties of Polymers", 2nd ed., Elsevier, Amsterdam, 1976.
(14) M. J. Richardson, P. J. Flory, and J. B. Jackson, *Polymer*, **4**, 221 (1963).
(15) W. S. Park and W. W. Graessley, *J. Polym. Sci., Polym. Phys. Eds.*, **15**, 85 (1977).
(16) G. Kraus and C. J. Stacy, *J. Polym. Sci., Part A-2*, **10**, 657 (1972).
(17) V. R. Raju, G. G. Smith, G. Marin, J. R. Knox, and W. W. Graessley, *J. Polym. Sci., Polym. Phys. Ed.*, **17**, 1183 (1979).
(18) V. R. Raju, E. V. Menezes, G. Marin, W. W. Graessley, and L. J. Fetters, *Macromolecules*, **14**, 1668 (1981).
(19) J. T. Gotro and W. W. Graessley, *Macromolecules*, preceding paper in this issue.
(20) J. M. Carella, Doctoral Thesis, Northwestern University, 1983.
(21) G. Kraus and J. T. Gruver, *Rubber Chem. Technol.*, **42**, 800 (1969).
(22) R. L. Arnett and C. P. Thomas, *J. Phys. Chem.*, **84**, 649 (1980).
(23) F. C. Stehling and L. Mandelkern, *Macromolecules*, **3**, 242 (1970); R. F. Boyer, *Macromolecules*, **6**, 288 (1973).
(24) R. Lam and P. Geil, *J. Macromol. Sci., Phys.*, **B20**, 37 (1981).
(25) J. J. Maurer, *Rubber Chem. Technol.*, **38**, 979 (1965).
(26) W. W. Graessley and S. F. Edwards, *Polymer*, **22**, 1329 (1981).
(27) P. J. Flory, "Statistical Mechanics of Chain Molecules", Wiley-Intersciences, New York, 1969.
(28) It is perhaps worth noting that $\nu L l^2 = 10$ is still well below the range required for liquid crystalline ordering of Kuhn steps in the undiluted polymers. Ordering of undiluted rods with aspect ratio x = length/diameter is predicted to occur for $x \gtrsim 6.4$.[29] With $l/2$ as the equivalent rod length[30] and $(4/\pi\nu L)^{1/2}$ as the rod diameter, $x = (\pi\nu L l^2/16)^{1/2}$ or $\nu L l^2 \gtrsim 200$ for ordering.
(29) P. J. Flory, *Proc. Natl. Acad. Sci. U.S.A.* **79**, 4510 (1982).
(30) P. J. Flory, *Macromolecules*, 11, 1141 (1978).
(31) G. Ronca, *J. Chem. Phys.* **79**, 1031 (1983).
(32) D. C. Prevorsek and B. T. De Bona, *J. Macromol. Sci., Phys.*, **B19**, 605 (1981).
(33) M. Doi and S. F. Edwards, *J. Chem. Soc., Faraday Trans. 2*, **74**, 1789, 1802 (1978).
(34) W. W. Graessley, *J. Polym. Sci., Polym. Phys. Ed.*, **18**, 27 (1980).
(35) I. D. Rudin, "Poly(1-butene)—Its Preparation and Properties", Gordon and Breach, New York, 1968.
(36) N. Hadjichristidis, X. Zhongde, L. J. Fetters, and J. Roovers, *J. Polym. Sci., Polym. Phys. Ed.*, **20**, 743 (1982).
(37) J. Mays, N. Hadjichristidis, and L. J. Fetters, *Macromolecules*, **1984**, *17*, 2723.
(38) C. J. Stacy and R. L. Arnett, *J. Phys. Chem.*, **77**, 78 (1973).
(39) W. W. Graessley, *Macromolecules*, **15**, 1164 (1982).

Structural Studies of Semifluorinated *n*-Alkanes. 1. Synthesis and Characterization of $F(CF_2)_n(CH_2)_mH$ in the Solid State

John F. Rabolt,* Thomas P. Russell, and Robert J. Twieg

IBM Research Laboratory, San Jose, California 95193. *Received March 16, 1984*

ABSTRACT: A series of semifluorinated *n*-alkanes, $F(CF_2)_n(CH_2)_mH$, has been synthesized as models for semiflexible polymers. In addition to the melting endotherm, DSC measurements indicate the presence of solid–solid phase transitions. Characterization of the molecular structure and the packing of chains in the crystal lattice in the room-temperature phase has been carried out by Raman spectroscopy, small-angle X-ray scattering (SAXS), and wide-angle X-ray diffraction (WAXD). Several possible packing structures consistent with these measurements are discussed.

Introduction

Fluorocarbon homopolymers have generated considerable interest due to their unique thermal, mechanical, and dielectric properties but little emphasis has been placed on characterization since fluoropolymers are usually insoluble in most common solvents and often crystallize in extended-chain morphologies, thus rendering them uncharacterizable by most common techniques.

Simultaneous optimization of the thermal and dielectric properties while attempting to improve the mechanical and solution characteristics has led to the copolymerization of fluorocarbon monomers with their hydrocarbon analogues. Thus, poly(vinylidene fluoride),[1] $(-CF_2CH_2-)_x$, and an E–TFE alternating copolymer,[2,3] $(-CF_2CF_2CH_2CH_2-)_x$, have become commercially available and possess high temperature stability, outstanding mechanical and dielectric properties and are soluble in a number of solvents. A variety of techniques have since been used to study the structure of these copolymers and a significant amount of information has been published detailing their structure in the solid state and in solution.[4–7] Similarly, theoretical studies[8,9] have also appeared using semiempirical atom–atom potentials to calculate minimum energy structures for both an isolated chain and the crystal lattice.

Unlike *n*-alkane oligomers, very few studies have been made of fluorocarbon oligomers because of the lack of availability of a series of high-purity materials. Dipole moments and conformational parameters for a series of α,ω-dihydroperfluoro-*n*-alkanes, $H(CF_2)_nH$ with n = 4, 6, 7, 8, and 10, were reported by Bates and Stockmayer[10] and later[11] expanded to include longer chains and $H(CF_2)_nI$ with n = 4, 6, and 8. Infrared and Raman studies[12,13] of short-chain perfluoro-*n*-alkanes, $F(CF_2)_nF$ with n = 4–6, have appeared while Raman studies[14,15] of the intermediate chain lengths have also been reported. As in the case of *n*-alkanes, the position of certain vibrational bands in perfluoro-*n*-alkanes was observed to vary as a function of chain length and thus was used to plot out portions of the phonon dispersion curves.[16] An overlay force field was then refined by using the finite molecule data and then applied

0024-9297/84/2217-2786$01.50/0

to the calculation of the vibrational spectrum of poly(tetrafluoroethylene) (PTFE).

On the basis of the unique structure and properties of alternating copolymers of the type $(-(CF_2)_n(CH_2)_m-)_x$, a series of semifluorinated n-alkanes, $F(CF_2)_n(CH_2)_mH$ (abbreviated FnHm), has been synthesized in order to investigate their structure and properties in the solid, solution and melt state in an attempt to predict the corresponding properties of their infinite chain analogues. In particular, it should be possible to design an alternating copolymer which has the high temperature stability approaching that of PTFE while at the same time maintaining the processability of polyethylene.

This work reports both the synthesis of a series of semifluorinated n-alkane diblock model compounds with varying segment lengths and the characterization of the chain conformation and the molecular packing in the crystalline state.

Experimental Section

Characterization. Differential scanning calorimetry (DSC) measurements were made on a Du Pont 1090 thermal analyzer. The melting points reported are the peak positions obtained from the second heating DSC trace of each material. The heating rate unless otherwise noted was 1 °C/min. The 90-MHz proton NMR spectra were obtained on a Varian EM-390 with internal Me_4Si standard, proton-decoupled 20.13-MHz carbon NMR spectra were obtained on an IBM Instruments, Inc., NR/80 Instrument with a capillary deuterium oxide lock, and the 75.34-MHz fluorine NMR spectra were obtained on the IBM NR/80 Instrument with deuteriochloroform lock. Analytical vapor phase chromatography was performed on a temperature-programmed Hewlett-Packard 5830A gas chromatograph with a 6 ft-10% QF-1 column, and mass spectra were obtained at Shrader Analytical Laboratories, Detroit, MI.

All Raman data were obtained by using a Jobin-Yvon HG-2S double monochromator equipped with a cooled RCA 31034A-02 photomultiplier tube connected to standard photon counting electronics. Powdered samples of the semifluorinated n-alkanes were melt crystallized into Pyrex capillaries and irradiated with the 488-nm line of a Spectra Physics 165-08 argon ion laser. Each spectrum was obtained at a resolution of 1.5–2.0 cm^{-1} by the coaddition of successive scans using a Nicolet 1180 data system. Unless otherwise noted, no electronic or digital smoothing was applied to any of the displayed Raman spectra.

SAXS measurements were obtained by using a slit-collimated Kratky camera modified for use with a one-dimensional position-sensitive detector (TEC210). Nickel-filtered copper radiation from a standard-focus Phillips tube operated at 40 kV and 20 mA was utilized as a source and the scattered radiation was discriminated electronically. The specimens investigated were powders packed into 1-mm diameter capillaries with 0.01-mm wall thickness. The data were corrected for parasitic scattering, detector homogeneity, and electronic noise in the standard manner. Desmearing calculations were not performed on the data; however, the effects of the finite beam and detector window sizes were incorporated into the calculations.

WAXD experiments were performed with a fine-focus Phillips copper tube operated at 50 kV and 20 mA. The measurements were conducted in the reflection mode on powder specimens rotating at 1 Hz with 1° divergence entrance and receiving slit apertures. The diffracted radiation was collected at 2θ increments of 0.05° by using a graphite monochromator followed by a scintillation detector with pulse height discrimination. The flight path from the X-ray tube to the detector was evacuated.

Synthesis. Although the synthetic procedure required to prepare the semifluorinated n-alkanes has been available for some time, little detailed information has appeared in the literature concerning the preparation and properties of any homologous series of the parent molecules. This is rather surprising considering the effort which has been devoted to the preparation of perfluoroalkyl derivatives of a variety of cyclic and polycyclic alkenes and numerous other functionalized linear olefins which have been studied for their surfactant and detergent properties. Of the semifluorinated n-alkanes studied herein, the F6H6 compound has been described[17] but no experimental details are available and the F8H8 compound was originally prepared by Bloechl.[18] A number of lower molecular weight semifluorinated n-alkanes have been prepared by Mahler but the data have only recently become available.[19]

Of the variety of techniques now available to couple the perfluoroalkyl and alkyl segments of these molecules, we have relied upon the now well-known process of free radical initiated addition of a perfluoroalkyl iodide to a terminal olefin as described by Brace.[20] In practice, the perfluoroalkyl iodide and an excess of liquid olefin are warmed until a homogeneous solution results and then AIBN initiator is added in small portions until the iodoperfluoroalkane is consumed; in the special case of the gaseous olefins, ethylene and 1-butene, a modification of the technique of Knell[21] was utilized. The iodine-containing intermediate was dehalogenated with zinc in boiling ethanol into which a stream of HCl gas was passed; in the case of the higher molecular weight intermediates where solubility was somewhat of a problem, n-octane was used as a cosolvent in the dehalogenation reaction. Both synthetic steps are very efficient and relatively free of side reactions except in the case of the dehydrogenation step in which a small quantity of higher molecular weight material, possibly a dimer, is sometimes formed. The ultimate purity of the semifluorinated n-alkane appears to be most strongly a function of the purity of the perfluoroalkyl iodide and α-olefin starting materials. Typically, the intermediate and final product are accompanied by traces of contaminants of very similar boiling point which makes separation by distillation without excessive losses in yield difficult. Also, the impurities are often not efficiently removed by recrystallization since their solubilities are very similar to the desired product. However, by a combination of simple fractional Kugelrohr distillation(s) and recrystallization(s), the materials used in this study have all been obtained in greater than 98% purity without resorting to the routine use of ultrapure standard olefins or purification techniques such as spinning band distillation or preparative vapor phase chromatography (vpc).

The synthesis and purification of 14-iodo-1,1,1,2,2,3,3,4,4,5,5,6,6,7,7,8,8,9,9,10,10,11,11,12,12-pentacosafluoroeicosane (F12H8I) and 1,1,1,2,2,3,3,4,4,5,5,6,6,7,7,8,8,9,9,10,10,11,11,12,12-pentacosafluoroeicosane (F12H8) are given in detail and are generally representative of the preparations used for the semifluorinated n-alkanes employed in this study.

F12H8I Preparation. In a 100-mL round-bottom flask equipped with stirbar, condenser, and nitrogen inlet were placed freshly distilled 1-octene (4.49 g, 40 mmol, Aldrich, 97%) and perfluorododecyl iodide (14.92 g, 20 mmol, Riedel-de Haen, 95%). The flask was warmed in a 100 °C oil bath and AIBN (50 mg total) was added to the stirred solution in 10 5-mg increments over the next 30 min. After the first few AIBN additions, a pink color due to free iodine persisted and the solution became homogeneous. After the final AIBN addition, the solution was maintained at 100 °C an additional 15 min and was then cooled to room temperature to give the product mixture as a pink wax. Excess olefin and low-boiling components were stripped off by Kugelrohr distillation (25–110 °C at ≥200 μm) and then the product fraction (115 °C at 180 μm to 150 °C at 60 μm) was collected as a colorless wax which was then crystallized from methanol/acetone to give 14.14 g (82%) of the product as a waxy white powder, vpc purity 97.2%; mp 95 °C; proton NMR (Freon TF) δ 0.70–1.10 (cr t, methyl, 3 H), 1.10–2.00 (br s with downfield sh, 10 H), 2.50–3.30 (m, $-CF_2CH_2CHI-$, 2 H), 4.10–4.50 (m, $-CF_2CH_2CHI-$, 1 H); carbon NMR (Freon TF) δ 33.17, 32.48 (t, J = 27), 30.59, 30.46, 23.85, 21.68, 21.52, 14.58 (nonfluorinated carbons only).

F12H8 Preparation. In a 1000-mL three-neck round-bottom flask equipped with stirbar, condenser, bubbler, and gas-dispersion inlet were placed the F12H8I intermediate (12.87 g, 15 mmol) and absolute ethanol (200 mL). The stirred solution was brought to a gentle boil, hydrogen chloride gas was admitted in a slow stream, and zinc powder (3.93 g, 60 mmol) was added in small portions (vigorous foaming) over the next 30 min. After all the zinc had been consumed, the solution was cooled to room temperature and transferred to a separatory funnel with the aid of hexane (250 mL) and water (250 mL). The phases were separated, and the organic phase was washed with water (250 mL) and saturated

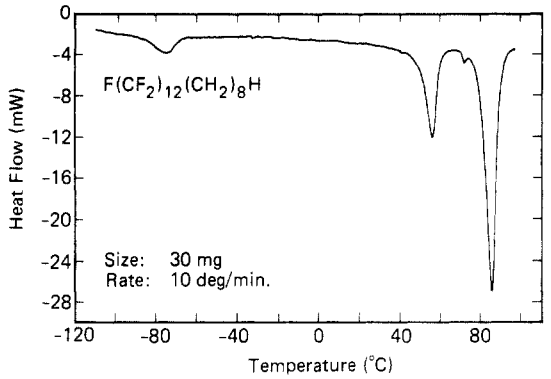

Figure 1. DSC trace of F12H8 recorded at a heating rate of 10 °C/min.

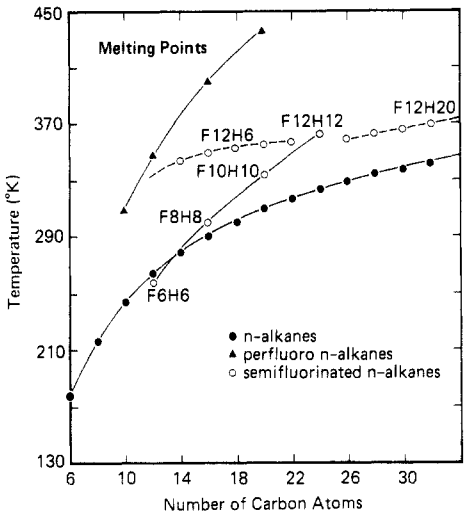

Figure 2. Plot of the melting points of F*n*H*m* as a function of the total number of backbone carbon atoms. For comparison, the melting points of *n*-alkanes (●) and perfluoro-*n*-alkanes (▲) have been included.

sodium bicarbonate solution (50 mL) and then dried over magnesium sulfate, filtered, and concentrated to a white solid by rotary evaporation. This material was purified by Kugelrohr distillation (25–130 °C, 500 μm) and the distillate crystallized from methanol/acetone to give the product as a white powder totalling 9.93 g (90%): vpc purity 98.4%; mp 82 °C; proton NMR (Freon TF) δ 0.70–1.06 (cr t, 3 H), 1.06–1.60 (br s) and 1.30–2.32 (sym m, 14 H total); carbon NMR (Freon TF) δ 43.84 (t, J = 21, C8), 47.97, 33.02, 31.03, 29.63, 23.87, 20.50, 14.68 (nonfluorinated carbons only); fluorine NMR ($CDCl_3$) δ 82.9 (t, J = 9.5, C_1F), 116.4 (s, $C_{12}F$), 123.8 (br s, $C_{4-10}F$), 124.7 (s, $C_{11}F$), 125.6 (s, C_3F), 128.1 (s, C_2F); mass spectrum, m/z (relativity intensity) 732 (M^+, 50%), 703 (100%).

Results and Discussion

Thermal Analysis. A typical DSC trace obtained at 10 °C/min from F12H8 is shown in Figure 1. In addition to the intense melting endotherm which occurs in the vicinity of 85 °C, there are two other weaker endotherms in the 40–80 °C range and an isolated broad peak at −75 °C. In the case of the former (those in the 40–80 °C range), optical microscopy was used in order to ascertain that these peaks were truly associated with solid–solid phase transitions. The nature and molecular mechanism of these transitions are beyond the scope of this current work but will be the subject of a forthcoming article.[22]

Figure 2 contains the peak melting points (in K) of three series of short-chain oligomers plotted against the total number of backbone carbon atoms. Included on this plot are *n*-alkanes, perfluoro-*n*-alkanes, and semifluorinated *n*-alkanes ranging in length from 6 to 32 backbone atoms.

Table I
Melting Points of Semifluorinated *n*-Alkanes

compd	T_m, °C	compd	T_m, °C
F6H6	−13.0	F12H8	82.0
F8H8	27.0	F12H10	84.0
F10H10	61.0	F12H12	89.0
F10H8	53.0	F12H14	86.0
F10H12	63.5	F12H16	90.0
F12H2	71.0	F12H18	92.0
F12H4	76.0	F12H20	96.0
F12H6	79.0		

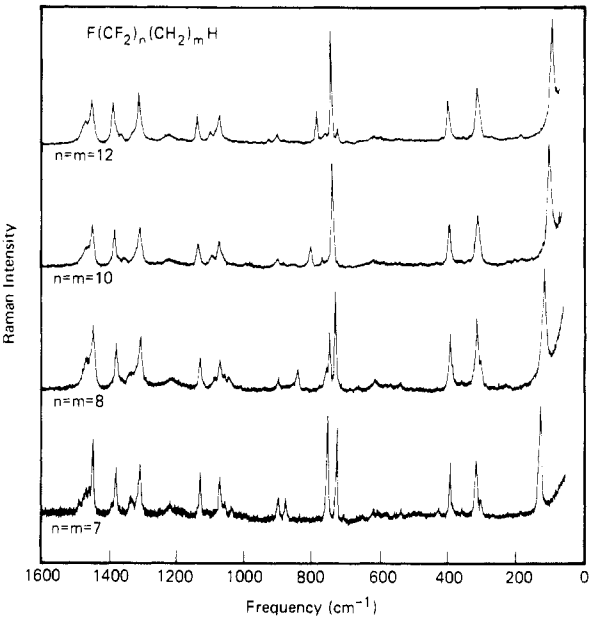

Figure 3. Raman spectra (20–1600 cm^{-1}) of semifluorinated *n*-alkanes having an identical number of $-CH_2-$ and $-CF_2-$ groups. Bandwidth was typically 1.5–2.0 cm^{-1}.

The former two are included for comparison with the semifluorinated oligomers. As shown, the melting points fall on at least three distinct curves with that for F*n*H*m*, where $n = m$, exhibiting the largest slope. The F12H*m* compounds with $m < 12$ appear to fall on one curve while for $m > 12$, i.e., longer hydrocarbon sequences, the melting point behavior appears to parallel that of the *n*-alkanes (lower curve). This would suggest at least three distinct modes of molecular packing each with unique intermolecular forces. Several of these will be discussed in connection with the SAXS data in a later section.

A complete set of melting points for all the compounds thus far studied appears in Table I.

Raman Spectroscopy. Although Raman measurements of semifluorinated *n*-alkanes in the melt have been reported,[23] no structural characterization of these materials in the solid state has appeared. Shown in Figure 3 are representative Raman spectra for the F*n*H*m* compounds where $n = m$. Similar spectra were obtained when $n < m$ and $n > m$. Since the intensity of Raman scattering is proportional to concentration, both hydrocarbon and fluorocarbon bands were identified by recording the spectra of compounds having different n/m ratios.

The strong bands in the 850–200-cm^{-1} region can be attributed to vibrations of the $-CF_2-$ groups. Upon careful examination of the asymmetric $-CF_2-$ stretching bands in the 700-cm^{-1} region, it is clear that the 730-cm^{-1} band falls at the same position in each spectrum and corresponds to a vibrational mode in which the $-CF_2-$ stretches on adjacent carbon atoms all occur in phase (i.e., $\phi = 0$). However, there are a number of other medium bands in this same region whose positions change as a function of the length

of fluorocarbon segment. An analogous observation has been made in perfluoro-*n*-alkanes[16] and *n*-alkanes, where it has been shown that in a simple model of a chain of identical oscillators with negligible end-group effects the solution of the secular equation is a function of only one variable, ϕ, the phase difference between identical displacements in adjacent oscillators, when the molecule undergoes a normal mode of vibration. For a chain of N oscillators, the solutions of the secular equation correspond to discrete values of the phase difference

$$\phi = k\pi/(N + 1) \qquad (k = 1, 2, ..., N) \qquad (1)$$

Hence, in the spectrum of an oligomer, it is possible to identify a series of bands corresponding to the same molecular motion and assign to each one a particular k value. When these bands have been assigned for a homologous series of oligomers, it is then possible to test their dependence on ϕ. A plot of frequency vs. phase angle should provide a smooth curve indicating that modes corresponding to this type of motion are a function of ϕ only. Once the actual shape of this dispersion curve is known, adjustment of the force field parameters so that the calculated dispersion curves will fit the experimental data can be undertaken. Although, in principle, this could be done for the fluorocarbon and hydrocarbon segments in the semifluorinated *n*-alkanes, there is one important difference. In the latter case, the N oscillators are not identical and furthermore contain one free end and one coupled end which would certainly affect the assignments of ϕ and thus the shape of the dispersion curves.

The region between 850 and 1500 cm^{-1} consists mainly of bands attributable to $-CH_2-$ vibrations with the exception of those at ~1380, 1296 (weak), and 1215 cm^{-1}. The CC stretching vibrations of an all-trans planar $-CH_2-$ structure are observed at 1060 and 1130 cm^{-1}, indicating that the hydrocarbon segment exists in the planar zigzag conformation in the solid state at room temperature. Additional information regarding the intermolecular environment and crystal packing of the hydrocarbon sequences is provided by the 1410–1460-cm^{-1} $-CH_2-$ bending region. Hendra et al.[25] have shown that both the number and relative intensity of bands in this region are indicative of the subcell packing of the $-CH_2-$ segments. Upon careful examination of this region in Figure 3, it becomes clear that the pattern of the $-CH_2-$ bending region in the $n = m$ semifluorinated *n*-alkanes (and in fact for all the compounds studied) is identical with that observed in the Raman spectrum of the "rotator" phase[26] of odd *n*-alkanes in which the subcell packing is hexagonal and the unit cell parameters sufficiently large to permit motion of the paraffin chain about its axis. Thus, this implies that the hydrocarbon segment of the semifluorinated *n*-alkanes does not close pack as in the polyethylene lattice but instead finds itself isolated from the adjacent hydrocarbon chains. This is further supported by studies of the CH stretching region (2700–3100 cm^{-1}), an example (F12H8) of which is illustrated in Figure 4. Here is shown the temperature behavior of the CH stretching region from −110 to 85 °C. As can be seen from the room-temperature (17 °C) spectrum, the band profile is a complex composite of CH stretching vibrations (both asymmetric and symmetric) originating from $-CH_3$ end groups, $-CH_2-$ paraffinic sequences, and the $-CH_2-$ group adjacent to the $-(CF_2)_nF$ sequence whose CH stretch is somewhat perturbed. The main feature of this figure is the striking similarity in low-temperature behavior with that observed for *n*-alkane urea clathrates.[27] In these mixed-crystal structures, the urea lattice forms a 5-Å channel into which *n*-alkane chains migrate during the crystallization process.

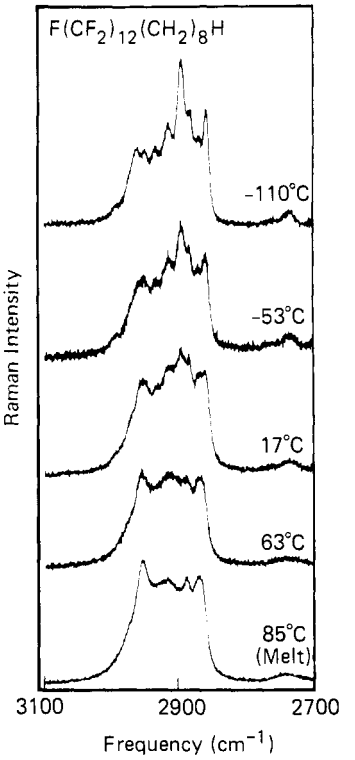

Figure 4. Raman spectra of the CH stretching region of F12H8 as a function of temperature.

This isolation of chains is manifested particularly in the CH stretching region due to the absence of intermolecular vibrational coupling. Thus, bands due to $-CH_2-$ stretching vibrations of the *n*-alkane clathrate are broad at room temperature due to the rotation and twisting of the hydrocarbon chain about its long axis. Both NMR[28] and thermal[29] measurements tend to support this type of motion. Upon lowering the temperature, a corresponding lattice contraction results and a restriction of the *n*-alkane motion due to intermolecular coupling occurs. Upon comparison of the temperature behavior of the CH stretching region in Figure 4 with that of the clathrate, it becomes apparent that the packing of the $-(CH_2)_8H$ segment is such that considerable molecular mobility occurs at room temperature. This conclusion is consistent with the previous result obtained from the $-CH_2-$ bending region.

In the region below 200 cm^{-1} are found vibrational bands characteristic of nonlocalized motions of the molecular backbone. As seen in Figure 3, this region is dominated by an intense band whose frequency increases with decreasing chain length, this behavior being reminiscent of that observed for the Raman-active longitudinal acoustical mode (LAM) observed in *n*-alkanes[30] and perfluoro-*n*-alkanes.[15] In these cases, the frequency of the LAM band was shown to vary inversely with chain length and was initially assigned to the accordion-like motion of the molecular backbone. The frequency–inverse chain length relationship led Mizushima and Shimanouti[30] to liken the molecular motion to the longitudinal oscillation of a uniform elastic rod. In this case, the expression relating frequency and the rod length is

$$\nu\ (cm^{-1}) = \frac{k}{2cL}\left(\frac{E}{\rho}\right)^{1/2} \qquad (2)$$

where c = speed of light, L = length of rod, E = Young's modulus of rod, ρ = density of rod, and k = integer 1, 2, ... In the molecular framework, L became the chain length

Frequency (cm^{-1}) of LAM-1

C_8H_{18}	$C_{16}H_{34}$	$C_8H_{17}C_8F_{17}$	C_8F_{18}	$C_{16}F_{34}$
234	148	106	135	74
$C_{10}H_{22}$	$C_{20}H_{42}$	$C_{10}H_{21}C_{10}F_{21}$	$C_{10}F_{22}$	$C_{20}F_{42}$
230	114	86	112	60

Figure 5. Comparison of the LAM-1 frequencies of FnHm with those of n-alkanes and perfluoro-n-alkanes having the same and half the number of backbone atoms.

while ρ is analogous to the crystalline density since the molecular chain axis (c axis) is parallel to the long axis of the rod and is in a crystalline environment. E corresponds to the axial Young's modulus of the long chain molecule while the integer, k, refers to the number of nodes in atomic displacement occurring during a particular LAM vibration. Since Raman intensity is proportional to the square of the change in polarizability with normal mode, only those modes with an odd number of nodes in atomic displacement are Raman active.

Although LAM in the n-alkanes and their perfluoro analogues involved the accordion-like motion of the entire backbone, it was not clear what the effect of appending a planar zigzag hydrocarbon chain to a helical fluorocarbon segment would be. In Figure 5, the LAM frequencies of semifluorinated n-alkanes are compared with that of oligomeric hydrocarbon and fluorocarbon chains having an identical ($n + m$) number and half the number of atoms in the backbone. Upon inspection, it becomes apparent that there is no decoupling of the LAM vibration at the junction of the planar zigzag and helical segments in the FnHm molecules. In fact, the observed frequency of F8H8, for example, was found to be halfway between that found for n-$C_{16}H_{38}$ and n-$C_{16}F_{38}$. Although this quantitative result is fortuitous, it does point out that the LAM band in the semifluorinated n-alkanes is a composite vibration involving both the planar zigzag and helical segments. This has recently been confirmed by the normal coordinate calculations of Minoni and Zerbi.[31] Using a simple coupled oscillator model with the point-mass approximation, they found that the LAM vibration of a diblock oligomer involved the molecular motion of both segments. Interestingly enough, when comparing the Cartesian displacements of each atom during the LAM-1 (LAM with one node in atomic displacement) vibration, they also found that the node in displacement occurred within the fluorocarbon segment independent of the length of the appended hydrocarbon chain for the range of lengths studied. Normal coordinate calculations using three-dimensional helical and planar zigzag structures are currently in progress in this laboratory in order to explore this interesting result in more detail.

A plot of LAM frequency vs. $1/(n + m)$, where $n + m$ is the total number of backbone atoms, is shown in Figure 6. In addition to the semifluorinated n-alkanes, data for the n-alkanes (Hm)[30] and the perfluoro-n-alkanes (Fn)[15] are also included. In all cases, a straight line intersecting the data points for each set of oligomers can be drawn which also intersects the origin as predicted by the uniform elastic rod model (see eq 2). In this simple model, the slope of the lines shown in Figure 6 is proportional to $(E/\rho)^{1/2}$, where E is the c-axis Young's modulus while ρ is the crystalline density. Since ρ decreases in the order Hn < FnHm < Fn, it is possible to at least qualitatively deduce that E for the FnHm (with $n = m$) oligomers is less than that of planar zigzag hydrocarbons but greater than that of helical fluorocarbon structures. Intuitively, this results because of the added freedom of rotation about bonds

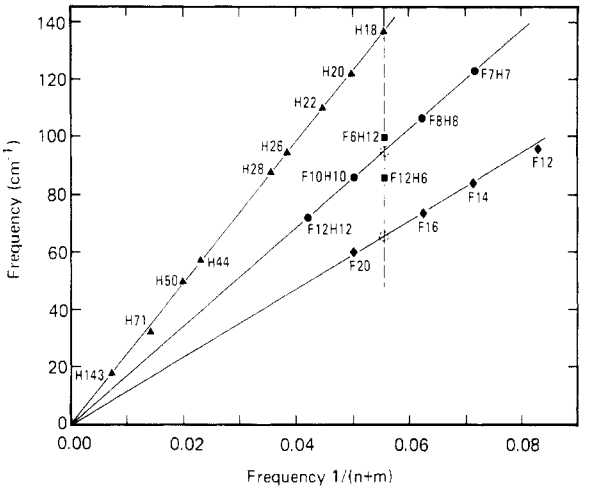

Figure 6. Plot of LAM-1 frequencies vs. the inverse of the total number of backbone atoms Fn = $F(CF_2)_nF$; Hm = $H(CH_2)_mH$.

which occurs in helical structures and inherently reduces the stiffness of helical chains relative to planar zigzag chains. It is apparent that composite chains containing both helical and planar segments will exhibit a Young's modulus intermediate between the extremes. This fact is further supported upon considering the vertical dashed line corresponding to a constant chain length found in Figure 6. In addition to data points found at the intersection of this line with that of each set of oligomers, the LAM frequencies for F6H12 and F12H6 also fall on this line since all have a total of 18 backbone atoms. However, beginning with F18 which exhibits a helical conformation and proceeding up this line, it becomes clear that decreasing the helical content of the oligomer (therefore increasing the planar zigzag content) causes an increase in modulus of the chain manifested by a subsequent increase in LAM frequency. This suggests the intriguing possibility of designing the conformational composition of an alternating copolymer such as to tailor its mechanical properties while maintaining desirable thermal and processing characteristics.

Small-Angle X-ray Scattering. Representative SAXS profiles of the semifluorinated n-alkanes are shown in Figure 7 for the F12Hm compounds indicated. The general shape of the SAXS was dependent upon the ratio of fluorinated to protonated carbon atoms. For $n/m \geq 2$, i.e., m = 2, 4, and 6, the SAXS consisted of one sharp reflection characteristic of one crystal packing. For $2 > m/n \geq 1$, i.e., for m = 8, 10, and 12, three to four maxima consisting of two first-order and one or two second-order reflections were observed. Consequently, two different crystal packings coexisted for these compounds at room temperature. For $n/m < 1$, i.e., for m = 14, 16, 18, and 20, a single sharp reflection was found. In addition, a diffuse maximum at smaller scattering vectors emerged as m increased from 14 to 20.

A composite diagram of the Bragg spacings corresponding to SAXS maxima as a function of the number of protonated carbons, m, for the F12Hm series is shown in Figure 8. Consistent with the DSC results and with the general appearance of the SAXS profiles, three distinct packings were observed depending upon the n/m ratio. An important feature of Figure 8 in terms of possible structures is the rate at which the spacings increase as the protonated sequence is lengthened. For $n/m \geq 2$, the magnitude of the spacings is slightly less than the length of the molecule, showing that the crystal thickness is limited by the length of a single molecule. Also, the Bragg

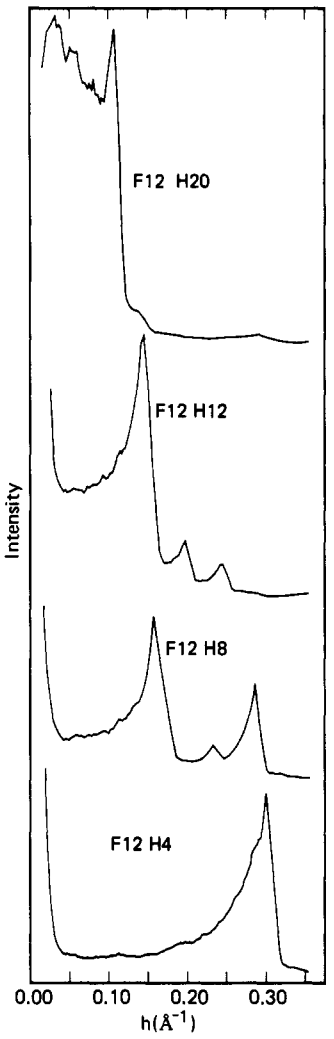

Figure 7. SAXS profiles for a series of semifluorinated *n*-alkane powders at room temperature.

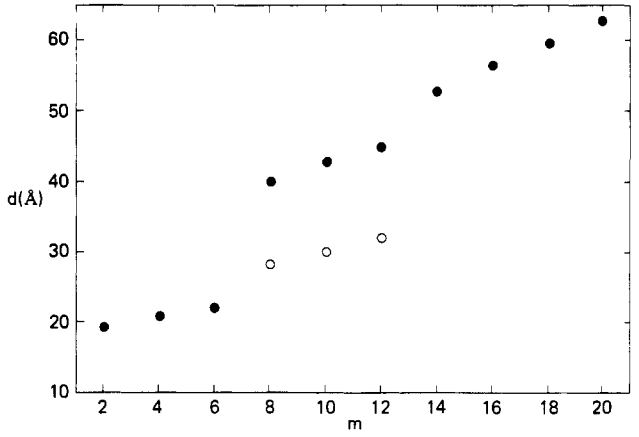

Figure 8. Bragg spacings corresponding to the peak maxima in the SAXS profiles. Full circles (●) represent the most intense first-order reflection observed whereas the open circles (○) indicate the presence of a weaker first-order reflection occurring in the same SAXS profile.

spacing increases less than 1.25 Å for each additional carbon added to the hydrocarbon segment. This would strongly suggest that the chains are tilted with respect to the crystal surface. For $2 < n/m \leq 1$, both spacings observed increase by 1.25 Å for each protonated carbon added to the molecule, indicating that the molecules pack perpendicular to the crystal surface. While the smaller spacing is given by the length of the molecule, the larger spacing is ca. 15 Å longer than the molecular length which corresponds to the length of a $(CF_2)_{12}$ unit. A possible structure that can account for this latter feature is one where the crystal is composed of two layers of molecules with overlapping hydrocarbon sequences. For $n/m < 1$, this "bilayer" type crystal packing can account for the spacings observed.

Unlike the *n*-alkanes or the perfluoro-*n*-alkanes, it is possible for the semifluorinated *n*-alkanes to assume several modes of packing in the crystal. Since hydrogen and fluorine have different electron densities, SAXS provides a means of evaluating the electron density profile of the crystal as well as the manner in which crystals stack with respect to one another. While absolute definition of the crystal structure can only be obtained from diffraction studies, the models generated from the SAXS calculations are useful in reducing the number of structures possible.

The slit-smeared SAXS, $I(\tilde{h})$, at a given scattering vector $h = (4\pi/\lambda) \sin(\epsilon/2)$ where λ is the wavelength and ϵ is the scattering angle is given by

$$I(\tilde{h}) = 2\int_0^\infty W_L(u) I(h^2 + u^2)^{1/2}\, du \qquad (3)$$

where $W_L(u)$ is the slit length weighting function. All structural information is contained within I(h) which is given by the Fourier transform of the correlation function, $\gamma(r)$. $\gamma(r)$ is given by

$$\gamma(r) = \frac{\langle \rho(x)\rho(x+r)\rangle}{\langle (\rho(x))^2\rangle} \qquad (4)$$

where the angled brackets indicate an average over all values of x. $\gamma(r)$ varies from 1 at $r = 0$ to 0 at $r = \infty$. $\rho(x)$ is the electron density as a function of distance x in the specimen which, in this study, is taken along the normal to the crystal surface. Knowing $\rho(x)$ for a given molecular packing within the crystal and the stacking of the crystals with respect to one another permits direct calculation of $I(\tilde{h})$ and comparison to the experimental results.

Best fits to the observed SAXS were obtained with the electron density profiles shown in Figure 9a,b. In all cases, voids ranging in size from 0–4 Å were placed between each crystal in developing a crystal stack. The total number of crystals in each stack varied from 10 to 50 with the scattered intensity from 50 such stacks being used to compare to the experimental data.

For $n/m \geq 2$, the SAXS could be adequately described by two different molecular packings. The first, called parallel packing, is where the fluorinated segments are aligned next to one another and the second, antiparallel packing, is where adjacent molecules are arranged to maximize the number of fluorine–hydrogen contacts. These are shown schematically in Figure 9a. Due to the size of the fluorine atoms, both structures would be consistent with the clathrate structure suggested by Raman results. Differentiation between these two different structures by SAXS was not possible due to the angular range over which the data were collected, the use of a powder specimen which prohibited absolute intensity measurements, and the tilt of the molecular axis away from the crystal normal. For $m = 2$, 4, and 6, the tilt angle between the molecular axis and the crystal surface normal calculated from the molecular length and crystal thickness was found to be ca. 10°, 21°, and 29°, respectively.

For $2 > n/m \geq 1$, two different structures were found to contribute to the scattering. Schematic diagrams and electron density profiles of these structures are shown in Figure 9b. As in the former series, an antiparallel packing structure was found. The origin of the scattering at lower scattering vectors can be described by the structure shown

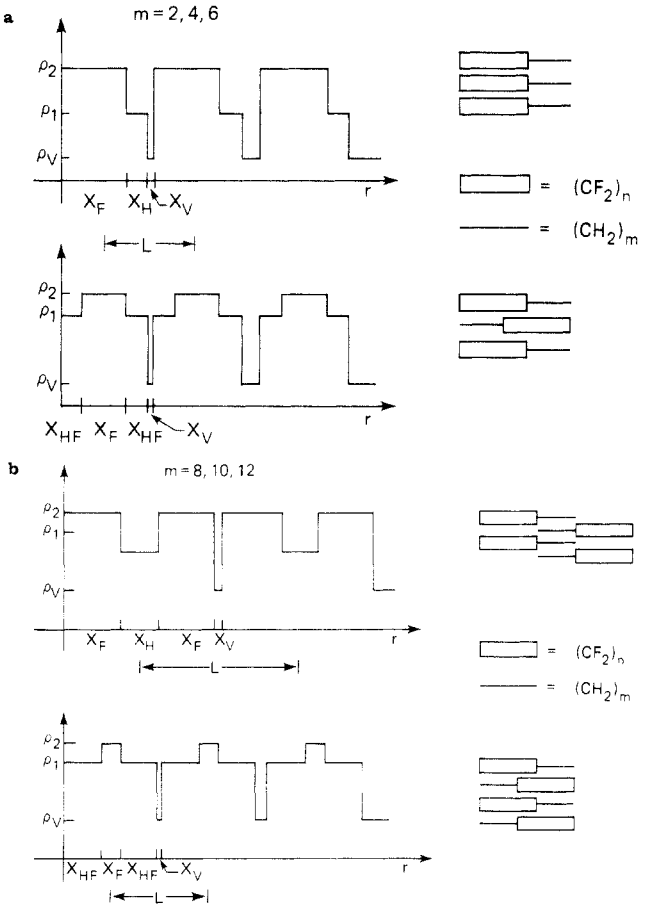

Figure 9. (a) Models for the electron density profiles of the F12H*m* compounds where $m = 2, 4$, and 6 as a function of distance r. X represents the length of the individual structures. The subscripts on H and F denote the protonated and fluorinated portions of the crystal, respectively; HF indicates a mixed section of the crystal; and V denotes a void. (b) Models for the electron density profiles of the F12H*m* compounds where $m = 8$, 10, and 12 as a function of distance, r.

in the upper part of Figure 9b. In this packing, two layers of parallel packed crystals interleave their hydrocarbon segments to form a crystal. This would adequately explain the observed long period and the change in the long period with increasing hydrocarbon length. It would also appear that the two structures are related to one another by simply sliding the molecule along its axis. This may also be the origin of the phase transitions observed in these materials below the melting point. Further work is in progress to elucidate this aspect.[22]

It is apparent that, at room temperature, the two structures are not present in equal concentrations. Shown in Figure 10 are the calculated scattering profiles for structures ranging from pure antiparallel (upper) to pure "bilayer" type crystal packing in number-fraction increments of 0.2 for F12H8. In comparison to the experimental data, it is apparent that the "bilayer" packing is the dominant structure at room temperature.

For $n/m < 1$, the single sharp maximum could be attributed to scattering arising from the "bilayer" type crystal packing. No evidence was found for the antiparallel packing. The origin of the broad maximum at lower scattering vectors is unknown at present.

Wide-Angle X-ray Diffraction. Diffraction spectra for n-$C_{19}H_{40}$, n-$C_{20}H_{42}$, n-$C_{12}F_{25}C_8H_{17}$ (F12H8), and n-$C_{20}F_{42}$ are shown in Figure 11. The spectra have been labeled with the (hkl) coordinates for n-$C_{20}H_{42}$ determined by Crissman et al.[32] and the ($00l$) coordinates for the remaining compounds that can be easily deduced from a

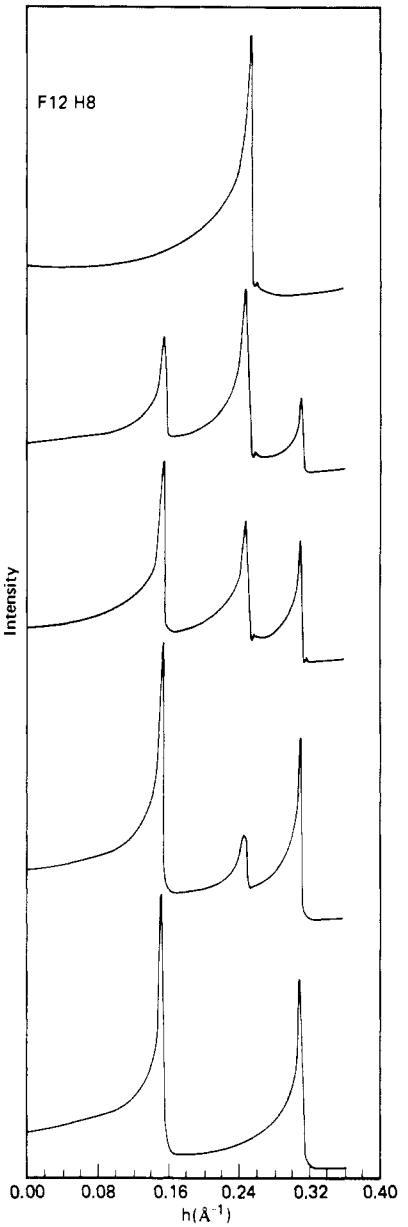

Figure 10. Calculated smeared SAXS profiles for F12H8 where the structure varied from pure "bilayer" type (lower) to a pure antiparallel (upper) crystal. The number fraction was varied in increments of 0.2.

casual observation of the diffraction patterns.[33-36] While it is not the intent of this section to fully index the spectra, the comparison presented in Figure 11 provides preliminary information concerning the FnHm compounds.

First, the F12H8 spectrum is much more complex than any of the other spectra shown. In addition to this, the ($00l$) spacings listed for F12H8 are continuations of the SAXS data represented earlier. The "a" form corresponds to the "bilayer" type crystal packing whereas the "b" form corresponds to the antiparallel packing forms. Definition of the intermolecular distances requires deciphering the actual crystal structure but it is quite clear from these data that the F12H8 differs drastically from either the triclinic[32] n-$C_{20}H_{42}$ or the orthorhombic[36] n-$C_{19}H_{40}$ alkane structures. It is evident that the intermolecular distances are governed predominantly by the fluorinated chain segment since the magnitude of these spacings resembles that of the n-$C_{20}F_{42}$. However, there are some significant differences. In particular, the F12H8 spectrum contains a strong reflection at 5.015 Å in comparison to the 4.935-Å reflection of the n-$C_{20}F_{42}$. This slightly increased spacing would be con-

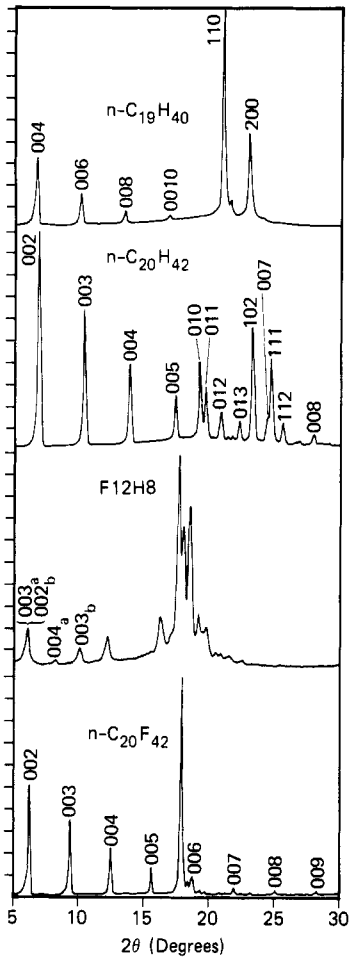

Figure 11. WAXD diagrams for n-$C_{19}H_{40}$, n-$C_{20}H_{42}$, n-$C_{12}F_{25}C_8H_{17}$ (F12H8), and n-$C_{20}F_{42}$ as indicated. The (hkl) indices shown are explained in the text.

sistent with the spectroscopic evidence of a rotator phase. Additional support for this is the diffuse nature of the F12H8 diffraction in comparison to that of the other compounds shown. Clearly, the diffraction results are consistent with the structures deduced from the scattering and spectroscopic data presented earlier.

Conclusions

A series of diblock semifluorinated n-alkane oligomers, $F(CF_2)_n(CH_2)_mH$, has been synthesized and characterized in the solid state. Thermal analyses indicate the presence of a solid–solid phase transition in addition to a crystalline melting point. A plot of melting points vs. chain length suggests at least three modes of packing in the crystal lattice.

Although Raman spectra above 200 cm^{-1}, where most motions are localized in specific molecular groups, can be considered a superposition of the spectrum of an oligomeric fluorocarbon with that of a short-chain n-alkane, below 200 cm^{-1} the Raman-active longitudinal acoustical mode (LAM) has been observed and shown to involve the accordion-like motion of both the hydrocarbon and fluorocarbon segments. In the CH stretch and $-CH_2-$ bending region of the spectra, Raman measurements indicated that the $-(CH_2)_mH$ sequences do not assume a close packing in the lattice as in the case of PE but instead exhibit considerable motional freedom similar to the "rotator" phase found in odd n-alkanes several degrees below their melting points.

WAXD studies supported this finding, revealing that the d spacings observed for the semifluorinated n-alkanes were intermediate between those found for fluorocarbons and hydrocarbons exhibiting either the orthorhombic or triclinic subcell structure. In addition, SAXS measurements provided additional information concerning the organization of chains in the crystal. For $n/m \geq 2$, it was found that the chains are tilted with respect to the lamellar surface, although differentiation between antiparallel or parallel packing of adjacent chains was not possible.

For $2 > n/m \geq 1$, two different possible crystal packings were found to coexist both having chains perpendicular to the lamellar surface. In this case, a crystal composed of two layers of interleaved molecules with overlapping hydrocarbon segments is present in addition to a crystal composed of chains adjacently packed end-to-end in an antiparallel arrangement.

When the hydrocarbon segment is longer than the fluorocarbon segment, i.e., $n/m < 1$, only bilayered interleaved structures can explain the experimental observations and the rigidity of the fluorocarbon helix represents a plausible argument for the existence of such structures in the solid state.

Studies of the implication of such crystalline arrangements on the mechanism of the solid–solid phase transition are currently in progress and will be the subject of a future publication.

Acknowledgment. We thank Grace Lim and Dr. William Parrish for providing the diffraction data, R. Siemens for assistance with the DSC experiments, and W. Fleming and C. Hrusa for the NMR measurements. We also acknowledge many helpful discussions with Professor B. L. Farmer (Washington State University) and Dr. W. Mahler (Du Pont).

References and Notes

(1) Naylor, R. E., Jr.; Lasoski, S. W., Jr. *J. Polym. Sci.* **1960**, *44*, 1.
(2) Clark, D. T.; Feast, W. J.; Ritchie, I.; Musgrave, W. K. R.; Modena, M.; Ragazzini, M. *J. Polym. Sci., Polym. Chem. Ed.* **1974**, *12*, 1049.
(3) Garbuglio, C.; Modena, M.; Valera, M.; Ragazzini, M. *Eur. Polym. J.* **1974**, *10*, 91.
(4) Lando, J. B.; Olf, H. G.; Peterlin, A. *J. Polym. Sci., Polym. Chem. Ed.* **1966**, *4*, 941.
(5) Cortili, G.; Zerbi, G. *Spectrochim. Acta, Part A* **1967**, *23A*, 285.
(6) Wilson, F. C.; Starkweather, H. W., Jr. *J. Polym. Sci., Polym. Phys. Ed.* **1973**, *11*, 919.
(7) English, A.; Garza, O. T. *Macromolecules* **1979**, *12*, 351.
(8) Farmer, B. L.; Hopfinger, A. J.; Lando, J. B. *J. Appl. Phys.* **1972**, *43*, 4293.
(9) Farmer, B. L.; Lando, J. B. *J. Macromol. Sci., Phys.* **1975**, *B11*, 89.
(10) Bates, T. W.; Stockmayer, W. H. *Macromolecules* **1968**, *1*, 12.
(11) Matsuo, K.; Stockmayer, W. H. *J. Phys. Chem.* **1981**, *85*, 3307.
(12) Piaggio, P.; Francese, P. G.; Masetti, G.; Dellepiane, G. *J. Mol. Struct.* **1975**, *26*, 421.
(13) Campos-Vallette, M.; Rey-Lafon, M.; Lagnier, R. *Chem. Phys. Lett.* **1982**, *89*, 189.
(14) Koenig, J. L.; Boerio, F. J. *J. Chem. Phys.* **1969**, *50*, 2823.
(15) Rabolt, J. F.; Fanconi, B. *Polymer* **1977**, *18*, 1258.
(16) Rabolt, J. F.; Fanconi, B. *Macromolecules* **1978**, *11*, 740.
(17) Clement, C.; Thoai, N. *C. R. Hebd. Seances Acad. Sci.* **1978**, *287*, 227.
(18) Bloechl, W. Neth. Appl. 6 506 069, 1969.
(19) Mahler, W. Du Pont Experimental Station, paper in preparation.
(20) Brace, N. O. *J. Org. Chem.* **1973**, *38*, 3167; *J. Org. Chem.* **1979**, *44*, 212.
(21) Knell, M. U.S. Patent 4 058 573, 1977.
(22) Russell, T. P.; Twieg, R. J.; Rabolt, J. F., in preparation.
(23) Twieg, R. J.; Rabolt, J. F. *J. Polym. Sci., Polym. Lett. Ed.* **1983**, *21*, 901.
(24) Snyder, R. G. *J. Mol. Spectrosc.* **1960**, *4*, 411.
(25) Hendra, P. J.; Jobic, H. P.; Marsden, E. P. *Spectrochim. Acta, Part A* **1977**, *33A*, 445.
(26) Barnes, J. D.; Fanconi, B. *J. Chem. Phys.* **1972**, *56*, 5190.
(27) Snyder, R. G.; Scherer, J. R.; Gaber, B. P. *Biochim. Biophys. Acta* **1980**, *601*, 47.
(28) Gilson, D. F. R.; McDowell, C. A. *Mol. Phys.* **1961**, *4*, 125.

(29) Pemberton, R. C.; Parsonage, N. G. *Trans. Faraday Soc.* **1965**, *61*, 2112.
(30) Mizushima, S.; Shimanouti, T. *J. Am. Chem. Soc.* **1949**, *71*, 1320.
(31) Minoni, G.; Zerbi, G. *J. Polym. Sci., Polym. Lett. Ed.* **1984**, *22*, 533.
(32) Crissman, J. M.; Passaglia, E.; Eby, R.; Colson, J. P. *J. Appl. Crystallogr.* **1970**, *3*, 194.
(33) Luth, H.; Nyburg, S. C.; Robinson, P. M.; Scott, H. G. *Mol. Cryst. Liq. Cryst.* **1974**, *27*, 337.
(34) Broadhurst, M. G. *J. Res. Natl. Bur. Stand. (U.S.)* **1962**, *66A*, 241.
(35) Doucet, J.; Denicolo, I.; Craievich, A. *J. Chem. Phys.* **1981**, *75*, 1523.
(36) Doucet, J.; Denicolo, I.; Craievich, A.; Collet, A. *J. Chem. Phys.* **1981**, *75*, 5125.

Viscoelastic Behavior of Concentrated Oil Solutions of Sulfo Polymers. 4. Magnesium Sulfo-EPDMs in Mixed Solvents

Pawan K. Agarwal,* Richard T. Garner, and Robert D. Lundberg

Exxon Research and Engineering Company, Corporate Research Science Laboratories, Annandale, New Jersey 08801. *Received June 29, 1983*

ABSTRACT: Concentrated solutions of magnesium sulfonated EPDMs in mixed solvents composed of paraffinic oils and alcohols have been characterized with respect to their viscoelastic behavior. It has been observed that the in-phase modulus is a strong function of time, especially in the low-frequency regime. The in-phase modulus increases substantially with time (at 23 °C), suggesting the formation of a progressively stronger network structure. Typically these systems require more than 10^4 s for an equilibrated system to form from which reproducible viscoelastic data can be obtained. Similar viscoelastic measurements were made at elevated temperatures, up to 75 °C. Aging behavior analogous to that at 23 °C was observed. In addition, it was observed that the in-phase modulus at low frequencies increased by a factor of 5 for a temperature change from 23 °C to 75 °C. This unusual increase in G' with increasing temperature is interpreted as an increase in the effective cross-link density at higher temperature due to changes in an equilibrium between the metal sulfonate groups and the alcohol cosolvent. These results demonstrate that, due to the exceptionally long relaxation times of these ionomer solutions, attempts to characterize such systems may be fruitless unless the systems are equilibrated either at high temperatures or after long periods of aging. The results at high temperatures demonstrate that the in-phase modulus of such systems can increase with temperature, in analogy with the viscosity behavior of such ionomer solutions. These results are all consistent with a more effective (stronger) ionic network occurring at high temperature or after longer aging times.

Introduction

In previous papers in this series[1-3] we have reported various aspects of the viscoelastic behavior of bulk EPDM and concentrated solutions of sulfonated EPDMs in a hydrocarbon solvent. When relevant, comparisons were made with the corresponding unfunctionalized base EPDM and with other high molecular weight polymers. These studies have shown that the viscoelastic behavior of the functionalized EPDM (ethylene–propylene–diene terpolymer) is a strong function of various variables: concentration, time, temperature, counterion, etc.

Among these variables the most remarkable effect is that of the counterion. We have observed that certain cations, e.g., magnesium and barium, have much stronger associating natures than others, e.g., zinc and ammonium. The outstanding associating nature of magnesium and barium is reflected in their sulfo-EPDM salts when dissolved in suitable nonpolar hydrocarbon solvents. These solutions, instead of forming a fluid having Newtonian characteristics (in certain limiting conditions), tend to form strong gels. Various measurements on as low a concentration as about 5 wt % sulfo-EPDM Mg salt (10 mequiv) in 100N[16] oil, up to greater than 250 °C above its glass transition, failed to exhibit any signs of viscous deformations. Some of these systems appear to form gels even at concentrations of about 1 wt %.

Theoretical studies of the process of gel formation of such ionomers have recently been attempted by Joanny[11] and Gonzalez.[12,13] Gonzalez,[13] following de Gennes'[14] ideas of the reptation of a chain in a permanently cross-linked gel and computations of the stress relaxation tensor of Doi and Edwards,[15] has derived viscoelastic functions of such ionomer gels which are qualitatively in agreement with the experiments.[2,3]

Among the strongly associative systems of the sulfonated polymer family, we have studied the magnesium salt of sulfo-EPDM in some detail and have observed various intriguing aspects of this material. Its high-temperature viscoelastic behavior appears to be unprecedented, having, to our knowledge, never been reported in the literature.[3] The gelation of sulfonated polymers generally appears to be a function of solvent, time, and temperature, and some aspects of these materials as a function of these variables are the subject of this paper.

Recently, Lundberg[4,5] characterized the dilute solution behavior of various kinds of metal sulfonated polymers. He observed that in mixed solvents the physical behavior of metal-neutralized sulfonated polymers is different from that of typical nonpolar polymers. His studies indicate that even strong physically associating systems, e.g., Mg salt of sulfo-EPDM in mixed-solvent systems, (apparently) form homogeneous solutions of low viscosities instead of forming gels of infinite viscosity. The viscosities of these solutions in mixed solvents, most often a hydrocarbon and an alcohol, are a strong function of concentration and the composition of the solvent mixture. It is interesting to observe the profound effects of small amounts of alcohols on the associations in these systems. The temperature–viscosity relationship of these systems is unusual[4] in that viscosities can increase substantially as temperature increases.

In this paper we report the viscoelastic behavior of sulfo-EPDM Mg salt (20 mequiv) in a mixed-solvent system.

Experimental Section

Solutions of magnesium sulfo-EPDM (20 mequiv)[10] at two concentration levels, 2.0 and 2.5 wt %, in 100N oil/hexanol[16] (98.5/1.5 by volume) were prepared. The magnesium sulfo-EPDM

0024-9297/84/2217-2794$01.50/0